

Accepted Manuscript

Journal of the Geological Society

A salty snapshot: extreme variations in basal erosion patterns preserved in a submarine channel

Junia Casagrande, David M. Hodgson & Jeff Peakall

DOI: <https://doi.org/10.1144/jgs2023-006>

To access the most recent version of this article, please click the DOI URL in the line above. When citing this article please include the above DOI.

Received 9 January 2023

Revised 3 November 2023

Accepted 18 December 2023

© 2024 The Author(s). This is an Open Access article distributed under the terms of the Creative Commons Attribution 4.0 License (<http://creativecommons.org/licenses/by/4.0/>). Published by The Geological Society of London. Publishing disclaimer: www.geolsoc.org.uk/pub_ethics

Manuscript version: Accepted Manuscript

This is a PDF of an unedited manuscript that has been accepted for publication. The manuscript will undergo copyediting, typesetting and correction before it is published in its final form. Please note that during the production process errors may be discovered which could affect the content, and all legal disclaimers that apply to the journal pertain.

Although reasonable efforts have been made to obtain all necessary permissions from third parties to include their copyrighted content within this article, their full citation and copyright line may not be present in this Accepted Manuscript version. Before using any content from this article, please refer to the Version of Record once published for full citation and copyright details, as permissions may be required.

A salty snapshot: extreme variations in basal erosion patterns preserved in a submarine channel

Authors: Junia Casagrande ^{1,2*}, David M. Hodgson¹, Jeff Peakall¹

¹Stratigraphy Group, School of Earth and Environment, University of Leeds, Woodhouse Lane, Leeds, LS2 9JT, England, UK

²Petrobras S. A., Avenida Henrique Valadares, 28, Rio de Janeiro, RJ, 20231-030, Brazil

Abstract: Active submarine channel bases are marked by large erosional features, such as knickpoints and plunge pools. Their presence in ancient channel-fills has rarely been documented, meaning their importance in submarine channel morphodynamics requires investigation. Using seismic reflection data calibrated by wells from a buried submarine channel-fill, we document erosional features 100s m long and 10s m deep, here interpreted as knickpoints and a plunge pool, and provide a mechanistic process for their transfer into the stratigraphic record for the first time. Channel incision patterns are interpreted to record a transient uplift in an otherwise subsiding depocentre. Local structural complexities in the channel slope formed zones of preferential scouring. A switch to a depositional regime preserved the irregular channel base inhibiting their upstream migration and smoothing of the channel base. Their formation and preservation record responses to salt tectonics and provide a unique snapshot of the formative processes of an ancient submarine channel. The presence of these exceptional basal scours indicates that headward erosion processes did not operate rapidly, challenging the paradigm that knickpoint migration controls channel evolution. Our results show that the primary erosion of the main channel surface, and long-term channel evolution, are dominated by far more gradual processes.

Submarine channels are primary long-term conduits for the delivery of terrigenous and anthropogenic particulates across continental slopes to the deep ocean floor (Carter, 1988; Hubbard et al., 2014; Kane and Clare, 2019). Their longitudinal profile and stratigraphic record are interpreted to reflect variations in slope gradient and flow properties (Pirmez et al., 2000; Kneller, 2003; Ferry et al., 2005; Covault et al., 2011).

Intrabasinal factors, such as tectonics (e.g., Gamberi and Marani, 2007; Heiniö and Davies, 2007; Georgiopoulou and Cartwright, 2013; Stright et al., 2017; Mitchell et al., 2021), mass transport deposits (Tek et al., 2021; Allen et al., 2022) or autogenic channel processes (Sylvester and Covault, 2016; Heijnen et al., 2020; Guiastrenec-Faugas et al., 2021), can perturb profiles and induce knickpoint development. The abrupt changes in channel floor gradient associated with knickpoints (Gardner, 1983; Heijnen et al., 2020) can increase flow velocity and turbulence, leading to hydraulic jumps (Komar, 1971), enhanced channel base scouring (Sumner et al., 2013; Dorrell et al., 2016), and eventually the formation of plunge pools (Gardner et al., 2020; Guiastrenec-Faugas et al., 2020, 2021). These erosional features produce uneven channel floor topography in modern deep-water environments (e.g., Bourget et al., 2011; Dalla Valle and Gamberi, 2011; Guiastrenec-Faugas et al., 2020, 2021; Gardner et al., 2020; Mitchell et al., 2021), which provide a snapshot of the formative processes of submarine channels (e.g., Heijnen et al., 2020). Geomorphic features associated with abrupt variations in channel gradient (i.e., knickpoints, plunge pools, crescentic bedforms) are considered highly dynamic and ephemeral (e.g., Heiniö and Davies, 2007; Hage et al., 2018; Guiastrenec-Faugas et al., 2020, 2021; Heijnen et al., 2020; Chen et al., 2021; Tek et al., 2021). Time-lapse seafloor mapping of active modern systems with sandy surficial sediments have documented headward erosion rates >100s metres per year (Guiastrenec-Faugas et al., 2020, 2021; Heijnen et al., 2020). Consequently, knickpoint migration has been argued to be the key driver of channel evolution in many submarine channel systems (Heijnen et al., 2020), rather than sediment redistribution by three-dimensional flow fields related to channel curvature (e.g., Peakall et al., 2007; Peakall and Sumner, 2015; Morris et al., 2022).

Through time, submarine channel profiles tend towards a smooth graded profile, which balances flow capacity and sedimentary load (e.g., Pirmez et al., 2000; Kneller, 2003; Gerber et al., 2009; Covault et al., 2011; Pettinga and Jobe, 2020). Consequently, preserved

submarine channel deposit thicknesses are constant longitudinally over 1-10s km (Di Celma et al., 2011; Macauley and Hubbard, 2013; Jobe et al., 2020), and relatively smooth profiles are assumed in numerical models (e.g., McHargue et al., 2011; Sylvester et al., 2011). A rare example of preserved scours has been documented in a buried Quaternary submarine channel-fill; these are <10 m deep and 300 m to 1 km in length (Snedden, 2013). However, the detailed processes and implications of such remnant scours have not been examined.

Here, we present a unique example of a buried submarine channel-fill that evolved above a dynamic stepped slope during the Oligocene-Miocene transition in the Campos Basin, offshore Brazil. The channel-fill preserves extreme longitudinal variations in basal erosion patterns (10s m deep, 100s m long), formed above a cohesive substrate. Seismic mapping and well data analysis were carried out in order to: (i) assess channel incision and thickness patterns and their relationship with underlying deposits; (ii) examine the channel-fill sedimentology, architecture and stratigraphy; (iii) propose mechanisms for the generation of local increased channel accommodation, ultimately recorded in exceptionally large and spatially variable channel thicknesses; and (iv) explain the generation and preservation of the incisional basal channel surface from an evolutionary perspective. We propose that the interaction of sediment gravity flows with a seafloor topography deformed by salt controlled the development and preservation of channel incision patterns.

Study area, data, and methods

The Campos Basin, offshore Brazil (Fig. 1), evolved from a rift during Gondwanan break-up (Jurassic/Lower Cretaceous) to a marine passive margin from the Albian to the present day (Chang et al., 1992; Fetter, 2009). We focus on a submarine channel-fill, informally named the Marlim Sul Channel (MSC; Fig. 1) (channel C2 of Casagrande et al., 2022), which incised sand-prone channel- and lobe-complexes deposited on a 40 km long stepped slope during the Oligocene-Miocene transition (Marlim Unit of Casagrande et al., 2022). The stepped slope configuration was controlled by extensional salt-tectonics, and the associated fragmentation of the Albian-Cenomanian carbonate-prone interval (raft tectonics) that overlies Aptian evaporites (Casagrande et al., 2022; Fig. 1A).

Through calibration with well data, the MSC-fill passes down dip from mud-prone deposits with low root mean square (RMS) amplitude values to sand-prone deposits with moderate to high RMS amplitude values (Casagrande et al., 2022). Here, we investigate the sand-prone channel-fill sector.

To document the basal surface and fill of the channel, two 3D high-resolution PSTM (pre-stack time migration) seismic reflection datasets were used. Acquisition parameters are: i) bin size 6.25 m for crossline and 12.5 m for inlines with 2 ms vertical sampling (approximate vertical resolution of 18 m), and ii) bin size 12.5 m for inlines and crosslines with 4 ms vertical sampling (approximate vertical resolution of 22 m). Both volumes are converted to the depth domain. Seismic reflection data were processed to zero-phase wavelet and are shown with SEG normal polarity. The Marlim Unit top is a trough with a negative reflection coefficient that indicates a decrease in acoustic impedance, whereas the base is a peak. Seismic interpretation was carried out using automatic and manual reflections tracking, and was calibrated by 24 wells with basic wireline logs (gamma-ray, density neutron, sonic and resistivity). Eight wells (two cored) intersect the MSC-fill. Seismic geomorphology was interpreted in an RMS amplitude map. Real thicknesses were obtained from a map of the top and base seismic horizons using the higher resolution depth converted seismic volume.

Longitudinal thickness variations of the channel-fill and the lobate features (LB and LC) were assessed by several measurements extracted from the thickness map and plotted graphically (Fig. 2). Within the channel-fill, the measurements are spaced every 400 m and were extracted at the thickest points of the channel cross-section. A total of 26 measurements were taken above the step; the same number was obtained in the lobate features. The 400 m distance was also used to plot the graph for LB and LC to match with channel measurements and facilitate comparison between thicknesses. Thickness values in the lobes were extracted between 500 m and 1000 m lateral to the MSC. Channel-fill stratigraphy was interpreted in a correlation panel along the MSC-fill based on well data and 3D seismic. The panel is hung from a laminated mudstone package observed in all the wells (see more in the channel-fill section).

The Marlim Sul Channel (MSC)

The MSC is readily observed in maps and profiles from seismic reflection data. Based on thickness patterns extracted between the mapped top and basal surfaces (reported by

average, minimum, and maximum depths, and the standard deviation (SD)), morphology and topographic configuration, the sand-prone channel sector is divided into three segments: corridor, step, and ramp (Fig. 1C) (Casagrande et al., 2022, see their figure 11). Abrupt longitudinal changes in channel-fill thicknesses are observed at three sites above the step (T1, T2 and T3), where the channel incises two sand-prone lobate features, LB and LC (Fig. 1C).

Corridor segment: The channel has very low sinuosity and constant width (300-350 m) (Fig. 1C). Average thickness is 56 m (41-75 m; 8 m SD). The channel cuts partially preserved linear high-amplitude anomalies, which well calibration shows to be sand-prone and 30 m thick.

Step segment: A salt-rooted synthetic normal fault, which cuts a carbonate raft, trends perpendicular to the channel course. The increased thickness and architectural changes across the fault support the interpretation of a break-in-slope between the corridor and step at the seafloor during the evolution of the Marlim Unit (Casagrande et al., 2022, fault marked in Fig. 1C and shown in map view and seismic profile in Fig. 3A and B). Above the step, the average channel-fill thickness is 52 m (26-86 m, 14 m SD). There are marked channel-fill thickness changes documented at bends T1, T2 and T3 (Figs. 1C and 2), which share similar thickness maxima and downstream lengths, but different characteristics and relationships to adjacent structural and stratigraphic elements. Channel width varies from 250 to 670 m and is wider at bends T1 and T2 (Fig. 1C). The channel is weakly sinuous across the step, apart from one pronounced bend at T3 (Fig. 1C).

Ramp segment: The distal part of the MSC is on the ramp, where the channel has a constant width (350 m wide) and is thinner than on the step and corridor (average 18 m, 11-36 m, 7.3 SD) (Figs. 1C and 2). The well-seismic calibration in the study area indicates that moderate to high seismic amplitudes relate to a sand-prone fill (Casagrande et al., 2022).

In summary, the average channel thickness data indicate that the channel-fill is thicker above the corridor and lower gradient step relative to the higher gradient ramp (Fig. 2). There are three prominent areas of anomalously thick channel-fills, T1, T2 and T3, which are examined in more detail below.

Relationship between the Marlim Sul Channel and older deposits

The break-in-slope at the step favoured the formation of the LB and LC distributary channel and lobe complexes (Casagrande et al., 2022). Low sinuosity high-amplitude seismic features in the corridor connect with LB and LC at the entrance of the step, which are interpreted as feeder channels (see white arrows in Fig. 1C). The MSC incised the corridor and step deposits between the feeder channels and the lobe complexes (Fig. 1C). Seismic mapping indicates truncation of reflections below the Marlim Unit, which is supported by thinner lobe thicknesses on average of LB (~20 m) and LC (~60 m) when compared with T2 thicknesses (Figs. 2 and 4). These observations support the complete removal of LB and LC beneath the MSC (see seismic inset in Fig. 1C) and deep incision below the lobes. A few metres of cores in some wells indicate that the rocks underlying the lobes and the channel-fill are laminated and bioturbated mudstones (Fig. 5E). Calibration with well logs in the cored wells and the well log patterns in several other wells show that the stratigraphy underlying the channel-fill and the lobes has higher gamma ray and density than the sand-prone deposits of LB and LC and the channel-fill itself (Fig. 6B), and a density and neutron logs cross over pattern (density log to the right and neutron to the left) suggesting non-reservoir facies. These mudstones form most of the deposits that were eroded by channel incision. There is a broad trend of decreasing channel thickness along the channel from the corridor to the ramp (Fig. 2). The magnitude of this decrease is 0.11° along the channel path (25 km), or 0.17° considering a straight measured distance of 17 km (Fig. 2). T1-3 punctuate this trend (Fig. 2). Notably, there is no significant change in channel thickness across the step-to-ramp transition.

Anomalously thick areas (T1-3)

The three anomalously thick channel-fill sites (T1-3; Figs. 1, 2, and 4) are all located on 'clockwise' orientated meanders on the step, and they have differing relationships to faults and adjacent deposits (LB and LC).

T1 is 1 km long and 350 m wide, and initially thickens downstream from 45 to 75 m in 350 m (average basal slope gradient: $\sim 5^\circ$; Fig. 4B1), and then thins from 75 to 45 m in 650 m (average basal slope gradient: 2.6°). Thickness patterns support T1 as a longitudinally asymmetric feature (Fig. 4B1). At T1, the channel around the bend is on average 150 m wider (maximum width of 550 m) than the corridor up-dip and also the next bend down-dip. T1 also coincides

with the break-in-slope at the up-dip edge of the step (Figs. 3, 4A and 4B1). The synthetic normal fault associated with the slope break is interpreted to have influenced T1 formation, and minor outboard faults do not show evidence of movement during the Marlim unit (Figs. 3, 4B2). Similar thickness increases are observed down-dip of the break-in-slope in the adjacent lobate features LB and LC (Fig. 4A), suggesting that the lobes and channel thicknesses record the same local accommodation control.

T2 is in the central part of the step, where the MSC thickens from 40 to 86 m over a downstream distance of 1 km ($\sim 2.6^\circ$ average gradient), then abruptly thins downstream to 32 m in 400 m (Figs. 2 and 4C1) forming an average counter slope of $\sim 8^\circ$. T2 also coincides with a wider (~ 650 m) and more sinuous channel segment compared to the immediately downstream channel bend that turns anticlockwise (~ 250 m) (Fig. 4A). The zone of thickest deposits is 1.4 km long and a maximum of 350 m wide (Fig. 4C1). Highly irregular channel edges are observed at the contact with LC (Fig. 4A, see black arrow). On the outer bend, T2 is partially bounded by a NW-SE normal fault (Figs. 3C, 4A and 4C2). At depth, the outer bend fault is salt-rooted and coincides with the edges of an underlying carbonate raft (Fig. 3C), and is mappable to the base of T2. The MSC reflections within T2 are rotated and thicken towards this fault (Fig. 4C2). The rotation and thickening of the reflections towards the salt-rooted fault suggests that it was active during the evolution of the MSC, and induced a local depression during channel incision. The geometry of the outer bend supports that the fault formed a synthetic listric fault segment as it propagated and widened towards the contemporaneous seafloor, as has been documented in exhumed systems (e.g., Hodgson and Haughton, 2004; Baudouy et al., 2021).

T3 is located on a tight bend in the MSC, 1.5 kilometres up-dip from the step-ramp slope break and thickens downstream in 1 km from 45-to-75 m (average gradient of $\sim 1.5^\circ$, Figs. 4A and 4D1), then thins from 75-to-40 m in 530 m (average gradient of $\sim 4^\circ$). The maximum width and length are 280 m and 1.6 km, respectively. The area of thickening is located at the centreline of the channel, not towards the outer bend. Overall, the bend displays similar upstream and downstream widths (~ 400 m). T3 is intersected by the same fault system present at T2 (Fig. 4A). The faults are parallel to the main channel orientation with a complex configuration that forms a graben, with T3 parallel to one of the bounding faults of the graben (Fig. 4D2). Thickening of the reflections above the Marlim Unit in the central low block of the graben

(Fig. 4D2, see pink arrows), and the lack of morphological changes in the bend across the faults suggest post-MSC fault movements. However, the reflections within T3 are rotated and thicken towards the outer bend, with onlapping reflections above T3 (Fig. 4D2). We interpret that the rotation and thickening of the reflections are due to a listric fault segment that parallels the outer bend of T3 (Fig. 4D2).

Channel fill sedimentology and stratigraphy

The sedimentology of the MSC-fill is constrained by cores from two wells (W2 and W8), which indicate a predominant fill of moderately sorted amalgamated structureless, fine-grained sandstones (Fig. 5), with subordinate medium- and rare coarse-grained sandstones. Well sorted fine-grained sandstones with plane-parallel lamination are secondary (Fig. 5). No coarse-grained or mud-clast-rich layers are observed within the channel-fill. Well logs motifs from gamma-ray and density/neutron are mainly blocky, which is compatible with the homogeneous character of the sandstones (Figs. 5 and 6).

Structureless sandstones record rapid deposition from turbulent high-density flows (Lowe, 1982). Traction in less dense flows interpreted from plane-parallel laminated sandstones is a subordinate process. The paucity of coarse-grained residual lags in the cores suggests depletive flows during channel filling.

In the upper part of the channel-fill, a unit characterised by the abrupt intercalation of sandstone beds with bioturbated laminated mudstones (Figs. 5 and 6), named the upper mud-prone package (UMP), is identified in all the wells above the step, suggesting longitudinal continuity (Fig. 6). The UMP culminates with a 3-5 m thick mudstone package (Figs. 5 and 6). Due to its fine-grained siliciclastic composition and crude lamination, the mudstones are interpreted as dilute turbidity current deposits (Talling et al., 2012), possibly with a minor contribution of background sedimentation. The UMP is interpreted to record a period of sand starvation. Abrupt changes from sandstone to mudstone facies in a channel-fill have been related to channel deactivation (Mutti and Normark, 1987). The impedance contrast between oil-saturated sandstones and the UMP permits seismic detection of the fine-grained package. Seismically, the top of the UMP coincides with a change in seismic polarity (a black peak indicates an increase in acoustic impedance due to a relatively higher density), which can be

tracked in the thickest parts of the channel-fill in the step and corridor (Fig. 6A, see white arrows).

The seismic profile along the channel-fill shows high-amplitude semi-parallel seismic reflections. In T2 and T3, well correlations support that the basal reflections likely pinchout against the channel base, suggesting that deposition was contained by the incisional surface (Fig. 6A). Towards the top of the channel-fill, there is greater reflection continuity, supported by well log correlations.

The longitudinal continuity permits the MSC-fill to be sub-divided into a lower sand-prone package (LSP), overlain by a fine-grained unit, the lower mud-prone package (LMP, up to 4 m thick; Fig. 6B). The LSP and LMP are interpreted to be the oldest preserved MSC-fill, with the LMP recording a regional reduction of sand supply. An overlying intermediate package (IP) comprises two sand-prone units intercalated with an interbedded (mudstones and sandstones) unit (Fig. 6B). Above the UMP is the upper sand-prone package (USP). Based on the correlation of the LSP and IP, we interpret that the USP is the only package recorded in the MSC-fill above the ramp (Fig. 6B).

The recognition of mud-prone and sand-prone stratigraphic packages supports waxing-to-waning sediment supply cycles during the fill of the MSC. The increased continuity of the stratigraphic packages suggests an aggradational pattern to the infill. Together, the evidence from the sedimentology and stratigraphy of the MSC supports passive filling without modification of the topographic irregularities at the base of the channel after infilling commenced.

Marlim Sul Channel (MSC) evolution

The incisional phase

The MSC architecture reveals a progressive increase in incision depth with distance up-dip, and three anomalously deep areas of incision that punctuate this trend. This pattern is contrary to that predicted by equilibrium slope concepts in above grade slopes, where deeper incision is expected across slope convexities such as the step-to-ramp break, and shallower incision or aggradation (e.g., channel-levee systems) are expected above low gradient areas

such as a step (e.g., Pirmez et al., 2000; Ferry et al., 2005; Deptuck et al., 2012; Shumaker et al., 2018). Here, we assess why this channel does not fit the standard model and examine the mechanics that caused the observed channel evolution.

There is a progressive longitudinal decrease in channel thickness, and thus incision, across the corridor, step, and ramp. Channel thickness, and consequently depth of incision, is greatest up-dip in the corridor (56 m) and step (52 m), and progressively decreases by 0.17° in a downslope direction towards the ramp (18 m). This suggests a primarily longitudinal deformation of the seafloor, and that the forcing mechanism operated on a considerably longer length scale than the scale of the observed ramps and steps. Furthermore, the channel is observed to incise below the adjacent lobes, and reach 50-60 m depth outside of T1-3. Given that channel widths are ~ 300 -670 m, then width:depth ratios are around 5-11, which represent low aspect ratios for primary submarine channels (e.g., Konsoer et al., 2013; Jobe et al., 2016; Shumaker et al., 2018), although they are similar to other heavily incised systems (e.g., Allen et al., 2022). The combination of progressive longitudinal change in incision, its continuity across ramps and steps, incision to well below the adjacent lobes, and the very narrow nature of the filled conduit, implies that there was pronounced uplift to drive channel incision. Furthermore, this uplift was greatest in the up-dip parts, diminishing down-dip, to primarily record a basinward tilt (Fig. 6). The uplift led to an increase in channel gradient (Fig. 2), resulting in enhanced incision. This relationship has been documented from morphometric analysis of submarine channels (e.g., Shumaker et al., 2018). However, here the incision is also linked to the total uplift, and because this increases up-dip, the maximum incision is higher in proximal locations. Despite the pronounced uplift, the 'stream power' (erosive power) of the submarine channel flows was sufficient to keep up with deformation in the case of an antecedent channel, or to regrade the slope in the case of channel propagation. Slope regrading by channel-forming processes, such as knickpoints and deep incision, has been demonstrated in other channel systems evolving above mobile slopes (e.g., Mayall et al., 2010; Kane et al., 2012; Jolly et al., 2017; Pizzi et al., 2023).

The exact cause of this deformation is challenging to determine in seismic reflection data. However, the study area is affected by salt tectonics, and associated syn-sedimentary slope deformation and tilting have been proposed to control the evolution of the Marlim Unit (Casagrande et al., 2022). Locally, the MSC is affected by salt-related faults, but the

progressive nature of this tilting across the corridor, step and ramp indicates that the uplift is related to movement on underlying structures at a greater wavelength and, therefore, likely from outside the study area.

The channel shows greater sinuosity on the step than in the corridor or ramp, suggesting that despite the overall longitudinal tilting, the subtle slope differences between these domains were sufficient to drive morphological change in the channel. The channel may have initiated and propagated through the area during or after the period of uplift, or it may have already formed prior to the uplift as an antecedent system. The lack of obvious bend amplitude growth during this incisional phase in bends T1-T3, which are characterised by near vertical channel thickness accumulation, suggests that the channel was present prior to the uplift.

A scoured channel base surface

The channel base is characterized by three exceptionally deep erosional areas (T1-T3), each ~1 km long, that have >20 m relief and up to ~40 m, with 1.5-5° average gradients on the up-dip scour surface, and 2.6-8° average gradients on the down-dip scour surface. These gradients are 1 to 2 orders of magnitude greater than the gradient calculated from the average longitudinal variation in channel thickness (0.17°). Whilst the original seafloor slope is hard to ascertain, the present seafloor slope in the study area of 1.5° may provide a broad guide, and this suggests that these up-dip scour gradients likely represent major increases in the original seafloor slope.

Controls on basal scour development

Here we concentrate on T1-3, kilometre-scale scours. However, the rugosity along this erosional surface is very high.

T1: The spatial association of T1 and high thickness patterns in the lobes (LB and LC) immediately downstream of the fault-controlled slope break (Figs. 3B, 4A) suggests a structural control in accommodation. Therefore, the fault controlling the slope break is interpreted to have been active during the deposition of the lobes and the evolution of the channel. The incisional feature is up to ~30 m deep, with a clear concavity, and extends down dip from the slope break for ~700 m, and up dip for ~300 m (Fig. 4B1). The concave

morphology of the scour, and its position close to the fault at the slope break, suggest that this is a channelised plunge pool (cf. Mitchell, 2006; Gardner et al., 2020; Guiastrenec-Faugas et al., 2020, 2021). Such plunge pools are observed to be quite short longitudinally (~ 50 m) as a function of channel width, W , ($\sim 0.33 W$) in recently deposited sandy substrates (Guiastrenec-Faugas et al., 2021). However, these can be longer (500-2000 m) and cover a wide range with respect to width (~ 0.16 - $2 W$) in more consolidated substrates, as might be expected in the example herein, given the magnitude of basal erosion (Mitchell, 2006; Gardner et al., 2020). T1 width is ~ 350 m, so a plunge pool of ~ 1 km length fits within the observed trends, albeit one of the most elongated relative to channel width (maximum 400 m) documented to date. Plunge pool depths in these stronger substrates can be up to 200 m for slope gradients of $\sim 3^\circ$ (Mitchell, 2006) or 100 m at slopes of $\sim 10^\circ$ (Gardner et al., 2020), with the former gradients more like the present-day seafloor gradient in the study area (1.5°). Such channelised plunge pools have been linked to the formation of hydraulic jumps (Mitchell, 2006; Sumner et al., 2013; Dorrell et al., 2016; Gardner et al., 2020; Guiastrenec-Faugas et al., 2020, 2021). The fact that the scour is observed to extend up dip beyond the slope break is consistent with observations at unconfined slope breaks where plunge pools extend into the slope (e.g., Lee et al., 2002; Hodgson et al., 2022).

T2: The deepest area of incision, up to 40 m greater than the average depths of incision, is around the bend apex across the central part of the channel, extending up-dip on the inner channel bend (Fig. 4C1). We interpret that the fault system at the outer bend of T2 (i.e., salt-rooted fault that bifurcates) led to the formation of a depression in the channel (Fig. 3). The magnitude of the depression, ultimately reflected in the anomalous thickness patterns of T2 and the rotation of the reflections (Fig. 4), suggests that the fault system was active during channel development, with rates of syn-sedimentary faulting in balance with channel-forming processes. The steep gradient at the upstream end of T2 records a knickpoint. This knickpoint may have undergone headward erosion around the bend, forming the present-day scoured surface. Channelised flows traversing knickpoints experience increased flow velocities driving substrate entrainment (Sumner et al., 2013; Dorrell et al., 2016), which explains deep scouring at T2. The channel widens to ~ 650 m here, partly reflecting that bend apices are wider than inflections (Palm et al., 2021), but also suggesting that the presence of the listric fault, and the associated scouring, broadened the channel.

T3: The erosional feature starts from the up-dip bend inflection point, and extends around the bend and past the apex. The maximum incision is >30 m above the average channel incision depths and is typically along the channel centreline, with the deepest area extending across at least half of the width of the channel (Fig. 4D1). The rotation and thickening of the MSC reflections towards the outer bend is evidence for syn-sedimentary activity of the listric fault segment during channel incision, forming a localised depression at the seafloor. As with T2, the up-dip part of the depression formed a knickpoint that may have undergone headward erosion up to the bend inflection.

T1, T2 and T3 represent local increases in channel depths during the incisional phase of the MSC. They are explained by the interaction of the flows with a complicated slope affected by salt-related faults, perpendicular (T1) or parallel (T2, T3) to the main flow direction. The formation of fault-related knickpoints and associated scours (T2, T3) and plunge pool (T1) are interpreted to have been preserved prior to large-scale knickpoint migration and smoothing of the channel base. These are rare examples of filled geomorphic features, which have been mostly documented in modern channels (Bourget et al., 2011; Dalla Valle and Gamberi, 2011; Guiastrennec-Faugas et al., 2020, 2021; Heijnen et al., 2020; Gardner et al., 2020), with a few examples of structurally controlled knickpoints preserved in buried channel systems (Adeogba et al., 2005; Stright et al., 2017). The scale of these reported knickpoints is similar to the features presented here. Nevertheless, the basal scours in the MSC are much larger than scours previously documented for submarine channels (maximum of 9 m for scour bends; Snedden, 2013). This study provides a comprehensive three-dimensional understanding of these features and explains their preservation.

The deformation associated with the development of large scours in the two bends, and the plunge pool at T1, was sufficiently rapid to lead to large-scale erosion, but slow enough to allow channel-forming processes to not be so disturbed that channel avulsion or crevasse splay development occurred (e.g., Casagrande et al., 2022). This suggests that the timescales of deformation and channel development are comparable. It is unknown whether fault-induced deformation in extensional salt-driven domains is typically in the same range as channel-forming processes, or whether this is an exceptional example.

A snapshot in time: the exceptional preservation of a scoured channel base surface

Given that the basal surfaces of submarine channels record long-term erosion and/or sediment bypass (e.g., Mutti and Normark, 1987; Deptuck et al., 2007; Hubbard et al., 2014; Hodgson et al., 2016) as channels tend to reach equilibrium, the formation of a smooth basal surface is expected (Sylvester et al., 2012; Hubbard et al., 2014). However, the preservation of kilometre-scale scours and a highly rugose basal surface suggests that the process of channel base smoothing was interrupted relatively soon after the formation of these features. Up-dip knickpoint migration of scours in T2 and T3 was limited, suggesting that the cessation of erosion was relatively rapid, or that the erosion rate declined sufficiently that further migration of knickpoints was reduced prior to full cessation of erosion. As the preserved geomorphic features scale with the basal channel surface, we interpret that the incision surface is the product of a single channel element (*sensu* Sprague et al., 2005; McHargue et al., 2011) and not a composite surface (i.e., not a channel complex). However, the channel-fill, with sand and mud-prone packages that reflect variations in the sediment supply, represents multiple waxing-and-waning cycles in sediment supply pointing to the fill being a composite body comprising several channel storeys (*sensu* Sprague et al., 2005). So, what caused the preservation of this snapshot of a basal surface prior to later smoothing? The cessation of erosion in this channel could have been related to several processes, including a rapid switch from uplift to subsidence, a change in flow properties leading to a change from erosion to deposition, or avulsion and complete or gradual channel abandonment. Avulsion can be dismissed here as the architecture of the MSC-fill records a passive style of deposition, much of it characterised by thick structureless sands indicative of the passage of high-density turbidity currents. Consequently, there is clear evidence that the channel stayed open and active long after the burial of the basal surface.

A return to subsidence after transient uplift would lead to the channel base moving towards a different longitudinal slope equilibrium marked by deposition to reduce the thalweg gradient. The incoming flows would have less erosive power and capacity to transport their load, thereby “fossilising” the thalweg morphology and producing the facies and stacking patterns interpreted in the MSC-fill. The interpreted transient and rapid salt-related uplift phase, with a basinward tilt, could have occurred during a longer period of overall subsidence, for example, due to a change in the mode of diapir growth (e.g., Jackson and Hudec, 2017)

and/or a change in tilt direction due to the application of a non-uniform load (e.g., Duffy et al., 2021). The length-scale of the basinward tilting is much longer than the length of the corridor-step-ramp. Therefore, the transient uplift is a far-field effect of salt tectonics beyond the study area and formed in the context of overall lateral tilting observed across a broader area (Casagrande et al., 2022) in this extensional salt domain. Furthermore, we interpret that the formation of several deep scours at the channel base is a function of syn-sedimentary faulting driven by underlying salt movement. Thus, a transient switch to uplift and reactivation of faults as a near-field response to far-field salt tectonics would be consistent with the dominance of salt tectonics on the evolution of this system. In Campos Basin, extensional reactivation of salt-rooted salt structures has been observed during the Oligocene and Miocene in the study area (e.g., Casagrande et al., 2022), and regional studies document salt tectonics activity during the Paleogene and Neogene as a response of transpression and transtension in basement structures (e.g., Fetter, 2009) and during the Paleogene due to the continuation of the regional thin-skinned extension (do Amarante et al., 2021).

Alternatively, a change in flow character could lead to the preservation of the channel base morphology. Reduction in flow magnitude, sediment concentration, or a change in sediment calibre to one with less fines (less efficient), or some combination of these, would result in flows that will be more depositional, raising the theoretical equilibrium profile (e.g., Kneller, 2003). Thus, at a given point in the system, there may be a change from flows being dominantly erosional to depositional. This change might have occurred through a relatively gradual change in boundary conditions linked to extra-basinal allocyclic controls such as sea-level variations (e.g., Deptuck et al., 2003), but is enough to pass a threshold from dominantly erosional to dominantly depositional (or non-erosional) flow behaviour. This scenario is likely supported by the channel cutting down to a harder, less erodible substrate, as already discussed, and the mantling of the channel base by harder to entrain material, like gravels or mud clasts. Initial changes in flow conditions may have acted to reduce erosion of the plunge pool and knickpoints, for instance, by a change from supercritical to subcritical flow regimes. Further changes in flow conditions would then progressively decrease the erosion rate before passing the threshold for deposition.

In summary, the preservation of the undulating channel base morphology, and lack of channel smoothing, could be linked to a return to subsidence after transient uplift, or a change in flow properties, or a combination of both factors.

Implications for knickpoint erosion and its influence on channel evolution

Observations of knickpoints and associated scours on the order of metres to >10 m in modern submarine channel systems and canyons have revealed that they can migrate upstream at rates of up to hundreds of metres per year (Guiastrennec-Faugas et al., 2020, 2021; Heijnen et al., 2020). This dynamism, and their impact on vertical and lateral erosion, have been used to argue that knickpoints control channel evolution (Heijnen et al., 2020). However, these observations of rapid knickpoint migration are in sandy, largely cohesionless sediments, within active channels. Here, we show an example of a channel cut into consolidated and cohesive mud-prone substrates. Whilst true timescales for erosion of this channel example are unknown, the fault-induced deformation occurs on timescales sufficiently slow that they do not induce channel avulsion, or other major channel planform changes (e.g., Holbrook and Schumm, 1999; Peakall et al., 2000). Furthermore, the knickpoints generated at T1-T3 have not had time to dissipate, whilst simultaneously smoothing the basal surface, something that takes place on decadal timescales in modern examples with cohesionless substrates (Guiastrennec-Faugas et al., 2020; Heijnen et al., 2020). Consequently, knickpoint migration in consolidated, cohesive, mud-prone substrates is likely associated with much slower migration rates than in modern sandy examples (see also Allen et al., 2022). This suggests that rapid knickpoint migration in weak substrates may not be representative of erosion during channel inception or long-term controls on channel evolution, but rather mark periodic overprint whose long-term stratigraphic record may be limited, and primarily recorded in the channel fill. The limited retreat of basal knickpoints observed herein suggests, in the generic case of submarine channels in consolidated mud-prone substrates (or equivalent high-strength substrates), that the long-term evolution of the basal geomorphic surface of a channel element is not primarily controlled by knickpoint erosion. Instead, channel evolution and bend development are likely controlled by the three-dimensional flow fields of traversing currents (e.g., Giorgio Serchi et al., 2011; Dorrell et al., 2013; Sumner et al., 2014), which in turn are related to channel curvature (e.g., Peakall and Sumner, 2015; Morris et al., 2022).

However, knickpoint migration likely play a key role in basinward reworking of sediment during aggradation of the conduit (Heijnen et al., 2020; Guiastrennec-Faugas et al., 2021).

Conclusion

The Marlim Sul channel comprises a rare example of a highly rugose submarine channel base preserved in an ancient system influenced by salt tectonics. The channel base contains geomorphic features considered ephemeral in modern systems, and dominated by three areas with anomalous (10s m) channel thicknesses. Channel incision patterns across the stepped profile are interpreted to reflect a salt-controlled transient uplift and basinward tilting of the slope. This scenario is controlled by a combination of far-field salt tectonics (a change to basinward tilt) and near-field salt tectonics (activation of listric faults), which is a scenario likely applicable to other evaporite-dominated basins worldwide. The singular preservation of these erosional features results from a combination of factors (salt tectonics, substrate strength, and/or flow and sediment supply) that induced changes in flow behaviour from erosional to depositional and inhibited headward knickpoint migration and channel base smoothing. The exceptional nature of this salt-generated basal scouring preserved in this ‘salty snapshot’ challenges the present paradigm that knickpoint migration dominates channel processes and evolution. Our results show that the primary erosion of the main channel surface, and long-term channel evolution, is much more gradualistic.

Figure 1. (A) Location map of Campos Basin and the study area within the Marlim Unit (blue polygon). (B) Strike seismic profile of the study area (time, 5x exaggeration, see D) showing the structural configuration associated with salt rollers and rafts. Several faults (white lines) crosscut the top Marlim Unit. The Lower Oligocene refers to the regional stratigraphic event Blue Marker (Winter et al., 2007). (C) Inset of seismic section in B, showing the MSC (in orange) cutting below the lobate features LB and LC (in yellow). (D) RMS amplitude map overlain by the thickness map of the Marlim Sul Channel (MSC). The slope sectors are marked in between red dotted lines (slope breaks). The slope break at the entrance of the step coincides with a fault. The high thickness areas (T1, T2, and T3) are marked in yellow circles above the step, where the channel cuts the lobate features LB and LC.

Figure 2. Graph showing longitudinal thickness variations along and parallel to the channel thalweg (across the corridor, step and ramp) and the lobate features LB and LC (across the step). Note the relationship between the areas of high channel thickness and lobes. The areas of locally increased thickness (T1-3) are marked in pale yellow. Note the overall downstream decrease in thickness and the limited incision at the step-to-ramp slope break. The average decrease in channel thickness values along the transect (green) from 63-to-13 m is used to calculate a gradient of 0.17°.

Figure 3. Large-scale structural control on the MSC (marked in white lines). (A) Seismic variance attribute map extracted from the top MSC horizon. Some of the faults in the area are indicated by yellow arrows, including the fault that controls the break-in-slope from the corridor to the step. T1-3 are marked on the map (for thicknesses see Fig. 4A). (B) Dip seismic profile, uninterpreted and interpreted, (higher resolution seismic volume, time domain, 5x vertical exaggeration, location in A), crossing the fault associated with the slope break between the corridor and the step. (C) Strike seismic profile, uninterpreted and interpreted, (higher resolution seismic volume, time domain, 5x vertical exaggeration, location in A) crossing T2. Note the structural configuration in the area with the fault at the edge of the carbonate raft affecting T2. This fault bifurcates (yellow arrow) forming a secondary fault at the outer bend of T2 (see text for explanation).

Figure 4. (A) Thickness map (m) of the lobate features (LB and LC) and the MSC-fill with main faults. Slope breaks in dotted pink lines (the slope break at the entrance of the step coincides with a fault). Channel geomorphology is marked by white dotted lines. Note the irregular channel edges marked with a black arrow. (B1) Detailed thickness map from T1. (B2) Dip seismic section crossing the slope break and longitudinally orientated in the T1 area. Note a main fault is associated with the slope break (yellow line) and other less important faults (dashed lines). All these faults are related to T1 formation. (C1) Detailed thickness map from T2. (C2) Strike seismic section crossing the T2 area. Note the close association of the yellow fault with T2 and how the base of the channel cuts underlying reflections at a deeper level than the lobes. (D1) Detailed thickness map of T3. (D2) Strike seismic section crossing the T3 area. Several faults form a graben. Pink arrows indicate variable thicknesses within this structure. The yellow fault is inferred as a structural control on T3. All the seismic profiles are shown in depth with 5x vertical exaggeration.

Figure 5. (A) MSC thickness map with well locations (W1-8), W2 and W8 have cores. The yellow line in the middle of the channel in the map refers to the seismic profile and the stratigraphic panel of Figure 5. (B) Well logs for W2; note the cored interval marked in pink. Stratigraphic packages marked in the well logs (intermediate package (IP), upper mudstone package (UMP), upper sandstone package (USP)). (C) Main sedimentary facies observed in the cores within the channel-fill, coloured circles indicate the position in the core boxes. (D1,2) Representative photographs of sedimentary facies in cores of W2 (sampled the IP and UMP). (E) Photograph of the bioturbated and laminated mudstones below the MSC. The green box shows the position in the log in B.

Figure 6. (A) Longitudinal seismic profile (depth domain, 5 x vertical exaggeration) along the MSC-fill (location in Figure 5A). Well calibration indicates that internal seismic reflections are related to the intercalation of sand- and mud-prone packages, although not all are resolved. Seismic reflections are, in general, semi-parallel and increase continuity stratigraphically. The upper mudstone package (UMP) top reflection is a peak; see white arrows. Note how this reflection is continuous along most of the channel-fill. (B) Stratigraphic panel calibrated by the wells and the seismic profile shown in A (with more vertical exaggeration). The channel-fill stratigraphy comprises sand-prone packages intercalated with mud-prone packages (lower sand-prone package (LSP), lower mudstone package (LMP), intermediate package (IP), UMP, upper sandstone package (USP)). These packages are depicted with an overall tabular geometry and are related to multiple sedimentary phases. The thickest mudstone unit of the UMP is used as the stratigraphic datum. The channel-fill stratigraphy and sedimentology are interpreted to reflect a passive style of deposition, with progressive healing of the channel base topography. The geometry of the beds within the packages is speculative since the beds are not observed in seismic data.

Figure 7. Marlim Sul Channel (MSC) incision across the stepped profile and above the lobate features and older mudstones. Pre-incision stage is shown in 1. Channels are expected to incise deeper across slope convexities, such as step-to-ramp slope breaks, and incise less across low gradient areas, such as steps. However, the incision patterns in the MSC are explained by an uplift stage (2), which increased the gradient and led to the whole area being above the equilibrium profile. The uplift magnitude decreases down dip (green arrows with different sizes). Consequently, differential vertical incision is produced as flows erode deeper across the corridor and step than above the ramp (3). By the end of the incisional phase, the sand-prone deposits related to the lobate features were removed as flows incised deep into the older mudstones; however, a graded profile was not achieved. For clarity, the

rugosity of the channel base surface is not represented (for which see Figure 2, and note that the y-axis in that figure is reversed relative to this figure, to highlight the channel rugosity, and the back-tilting).

References

Adeogba, A.A., McHargue, T.R. and Graham, S.A. 2005. Transient fan architecture and depositional controls from near-surface 3-D seismic data, Niger Delta continental slope. *AAPG Bulletin*, **89**, 627–643. <https://doi.org/10.1306/11200404025>

Allen, C., Gomis-Cartesio, L.E., Hodgson, D.M., Peakall, J. and Milana, J.P. 2022. Channel incision into a submarine landslide on a Carboniferous basin margin, San Juan, Argentina: Evidence for the role of knickpoints. *The Depositional Record*, **8**, 628–655, <https://doi.org/10.1002/dep2.178>

Baudouy, L., Haughton, P.D. and Walsh, J.J., 2021. Evolution of a fault-controlled, deep-water sub-basin, Tabernas, SE Spain. *Frontiers in Earth Science*, **9**, 767286.

Booth, J.R., Dean, M.C., DuVernay, A.E.III. and Styzen, M.J. 2003. Paleo-bathymetric controls on the stratigraphic architecture and reservoir development of confined fans in the Auger Basin: Central Gulf of Mexico slope. *Marine and Petroleum Geology*, **20**, 563–586.

Bourget, J., Zaragosi, S., Ellouz-Zimmermann, N., Mouchot, N., Garlan, T., Schneider, J.L., Lanfumey, V. and Lallemand, S. 2011. Turbidite system architecture and sedimentary processes along topographically complex slopes: the Makran convergent margin: The Makran turbidite system. *Sedimentology*, **58**, 376–406. <https://doi.org/10.1111/j.1365-3091.2010.01168.x>

Carter, R.M. 1988. The nature and evolution of deep-sea channel systems. *Basin Research*, **1**, 41-54.

Casagrande, J., Hodgson, D.M., Peakall, J. and Benac, P.M. 2022. Fill-and- Spill, Tilt-and- Repeat (FaSTaR) cycles: Stratigraphic evolution above a dynamic submarine stepped slope. *Basin Research*, **34**, 2162-2188, <https://doi.org/10.1111/bre.12700>

Chang, H.K., Kowsmann, R.O., Figueiredo, A.M.F. and Bender, A. 1992. Tectonics and stratigraphy of the East Brazil rift system: An overview. *Tectonophysics*, **213**, 97–138.

Chen, Y., Parsons, D.R., Simmons, S.M., Williams, R., Cartigny, M.J., Hughes Clarke, J.E., Stacey, C.D., Hage, S., Talling, P.J., Azpiroz-Zabala, M. and Clare, M.A. 2021. Knickpoints and crescentic bedform interactions in submarine channels. *Sedimentology*, **68(4)**, 1358-1377.

Covault, J.A., Fildani, A., Romans, B.W. and McHargue, T. 2011. The natural range of submarine canyon-and-channel longitudinal profiles. *Geosphere*, **7**, 313-332. <http://dx.doi.org/10.1130/GES00610.1>.

Dalla Valle, G. and Gamberi, F. 2011. Slope channel formation, evolution and backfilling in a wide shelf, passive continental margin (northeastern Sardinia slope, central Tyrrhenian Sea). *Marine Geology*, **286**, 95–105, <https://doi.org/10.1016/j.margeo.2011.06.005>

Deptuck, M.E., Steffens, G.S., Barton, M. and Pirmez, C. 2003. Architecture and evolution of upper fan channel-belts on the Niger Delta slope and in the Arabian Sea. *Marine and Petroleum Geology*, **20(6)**, 649-676, <https://doi.org/10.1016/j.marpetgeo.2003.01.004>

Deptuck, M.E., Sylvester, Z., Pirmez, C. and O'Byrne, C. 2007. Migration–aggradation history and 3D seismic geomorphology of submarine channels in the Pleistocene Benin-major Canyon, western Niger Delta slope. *Marine and Petroleum Geology*, **24**, 406–433, <https://doi.org/10.1016/j.marpetgeo.2007.01.005>

Deptuck, M.E., Sylvester, Z. and O'Byrne, C. 2012. Pleistocene seascape evolution above a “simple” stepped slope–Western Niger Delta. In: Prather, B.E., Deptuck, M.E., Mohrig, D. C., Van Hoorn, B. and Wynn, R.B. (eds) *Application of the Principles of Seismic Geomorphology to Continental-Slope and Base-of-Slope Systems: Case Studies from Seafloor and Near-seafloor Analogues*. SEPM Special Publication, **99**, 199–222, <https://doi.org/10.2110/pec.12.99>

Di Celma, C.N., Brunt, R.L., Hodgson, D.M., Flint, S.S. and Kavanagh, J.P. 2011. Spatial and temporal evolution of a Permian submarine slope channel–levee system, Karoo Basin, South Africa. *Journal of Sedimentary Research*, **81(8)**, 579-599, <https://doi.org/10.2110/jsr.2011.49>

do Amarante, F.B., Jackson, C.A.-L., Pichel, L.M., Scherer, C.M.S. and Kuchle, J. 2021. Pre-salt rift morphology controls salt tectonics in the Campos Basin, offshore SE Brazil. *Basin Research*, **33**, 2837–2861. <https://doi.org/10.1111/bre.12588>

Dorrell, R.M., Darby, S.E., Peakall, J., Sumner, E.J., Parsons, D.R. and Wynn, R.B. 2013. Superelevation and overspill control secondary flow dynamics in submarine channels. *Journal of Geophysical Research – Oceans*, **118**, 3895-3915, doi:10.1002/jgrc.20277

Dorrell, R.M., Peakall, J., Sumner, E.J., Parsons, D.R., Darby, S.E., Wynn, R.B., Özsoy, E. and Tezcan, D. 2016. Flow dynamics and mixing processes in hydraulic jump arrays: Implications for channel-lobe transition zones. *Marine Geology*, **381**, 181–193, <https://doi.org/10.1016/j.margeo.2016.06.005>

Duffy, O.B., Dooley, T.P., Hudec, M.R., Fernandez, N., Jackson, C.A.L. and Soto, J.I. 2021. Principles of shortening in salt basins containing isolated minibasins. *Basin Research*, **33(3)**, 2089-2117, <https://doi.org/10.1111/bre.12550>

Ferry, J.N., Mudler, T., Parize, O. and Raillard, S. 2005. Concept of equilibrium profile in deep-water turbidite systems: Effects of local physiographic changes on the nature of sedimentary processes and the geometries of deposits. In: Hodgson D.M. and Flint, S.S. (eds) *Submarine Slope Processes and Products*: Geological Society (London) Special Publication, **244**, 181–193.

Fetter, M. 2009. The role of basement tectonic reactivation on the structural evolution of Campos Basin, offshore Brazil: Evidence from 3D seismic analysis and section restoration. *Marine and Petroleum Geology*, **26**, 873–886, <https://doi.org/10.1016/j.margeo.2008.06.005>

Gamberi, F. and Marani, M. 2007. Downstream evolution of the Stromboli slope valley (southeastern Tyrrhenian Sea). *Marine Geology*, **243**, 180-189, <https://doi.org/10.1016/j.margeo.2007.05.006>

Gardner, T.W. 1983. Experimental study of knickpoint and longitudinal profile evolution in cohesive, homogeneous material. *Geological Society of America Bulletin*, **94(5)**, 664–672. [https://doi.org/10.1130/0016-7606\(1983\)94<664:ESOKAL>2.0.CO;2](https://doi.org/10.1130/0016-7606(1983)94<664:ESOKAL>2.0.CO;2)

Gardner, J.V., Peakall, J., Armstrong, A.A. and Calder, B.R. 2020. The Geomorphology of Submarine Channel Systems of the Northern Line Islands Ridge, Central Equatorial Pacific Ocean. *Front. Earth Sci.*, **8:87**, <https://doi.org/10.3389/feart.2020.00087>

Georgiopoulou, A. and Cartwright, J.A. 2013. A critical test of the concept of submarine equilibrium profile. *Mar. Pet. Geol.*, **41**, 35–47, <https://doi.org/10.1016/j.marpetgeo.2012.03.003>

Gerber, T.P., Amblas, D., Wolinsky, M.A., Pratson, L.F. and Canals, M. 2009. A model for the long-profile shape of submarine canyons. *Journal of Geophysical Research: Earth Surface*, **114**, F03002, doi:10.1029/2008JF001190.

Giorgio Serchi, F., Peakall, J., Ingham, D.B. and Burns, A.D. 2011. A unifying computational fluid dynamics investigation on the river-like to river-reversed secondary circulation in submarine channel bends. *Journal of Geophysical Research – Oceans*, **116**, C06012. doi:10.1029/2010JC006361

Guiastrennec-Faugas, L., Gillet, H., Jacinto, R.S., Dennielou, B., Hanquiez, V., Schmidt, S., Simplet, L. and Rousset, A. 2020. Upstream migrating knickpoints and related sedimentary processes in a submarine canyon from a rare 20-year morphobathymetric time-lapse (Capbreton submarine canyon, Bay of Biscay, France). *Marine Geology*, **423**, 106143, <https://doi.org/10.1016/j.margeo.2020.106143>

Guiastrennec-Faugas, L., Gillet, H., Peakall, J., Dennielou, B., Galliot, A. and Jacinto, R.S. 2021. Initiation and evolution of knickpoints and their role in cut-and-fill processes in active submarine channels. *Geology*, **49(3)**, 314–319, <https://doi.org/10.1130/G48369.1>

Hage, S., Cartigny, M.J., Clare, M.A., Sumner, E.J., Vendettuoli, D., Clarke, J.E.H., Hubbard, S.M., Talling, P.J., Lintern, D.G., Stacey, C.D. and Englert, R.G. 2018. How to recognize crescentic bedforms formed by supercritical turbidity currents in the geologic record: Insights from active submarine channels. *Geology*, **46(6)**, 563-566.

Heijnen, M.S., Clare, M.A., Cartigny, M.J.B., Talling, P.J., Hage, S., Lintern, D.G., Stacey, C., Parsons, D.R., Simmons, S.M., Chen, Y., Sumner, E.J., Dix, J.K. and Hughes Clarke, J.E. 2020. Rapidly-migrating and internally-generated knickpoints can control submarine channel evolution. *Nature Communications*, **11:3129**, <https://doi.org/10.1038/s41467-020-16861-x>

Heiniö, P. and Davies, R.J. 2007. Knickpoint migration in submarine channels in response to fold growth, western Niger Delta. *Marine and Petroleum Geology*, **24**, 434–449, <https://doi.org/10.1016/j.marpetgeo.2006.09.002>

Hodgson, D.M. and Haughton, P.D. 2004. Impact of syndepositional faulting on gravity current behaviour and deep-water stratigraphy: Tabernas-Sorbas Basin, SE Spain. In: Lomas, S.A. and Joseph, J. (eds) *Confined Turbidite Systems*. Geological Society, London, Special Publications, **222**, 135-158.

Hodgson, D.M., Kane, I.A., Flint, S.S., Brunt, R.L. and Ortiz-Karpf, A. 2016. Time-transgressive confinement on the slope and the progradation of basin-floor fans: Implications for the sequence stratigraphy of deep-water deposits. *Journal of Sedimentary Research*, **86(1)**, 73-86.

Hodgson, D.M., Peakall, J. and Maier, K. 2022. Submarine channel mouth settings: processes, geomorphology, and deposits. *Frontiers in Earth Science*, **10:790320**, <https://doi.org/10.3389/feart.2022.790320>

Holbrook, J. and Schumm, S.A. 1999. Geomorphic and sedimentary response of rivers to tectonic deformation: a brief review and critique of a tool for recognizing subtle epirogenic deformation in modern and ancient settings. *Tectonophysics*, **305**, 287-306.

Hubbard, S.M., Covault, J.A., Fildani, A. and Romans, B.W. 2014. Sediment transfer and deposition in slope channels: deciphering the record of enigmatic deep-sea processes

from outcrop. *Geological Society of America Bulletin*, **126(5-6)**, 857-871, <https://doi.org/10.1130/B30996.1>

Jackson, M.P.A. and Hudec, M.R. 2017. *Salt Tectonics: Principles and Practice*. Cambridge University Press, Cambridge, <https://doi.org/10.1017/9781139003988>

Jobe, Z.R., Howes, N.C. and Auchter, N.C. 2016. Comparing submarine and fluvial channel kinematics: implications for stratigraphic architecture. *Geology*, **44**, 931–934, <https://doi.org/10.1130/G38158.1>

Jobe, Z.R., Howes, N.C., Straub, K.M., Cai, D., Deng, H., Laugier, F.J., Pettinga, L.A. and Shumaker, L.E. 2020. Comparing aggradation, superelevation, and avulsion frequency of submarine and fluvial channels. *Frontiers in Earth Science*, **8:53**, <https://doi.org/10.3389/feart.2020.00053>

Jolly, B.A., Whittaker, A.C. and Lonergan, L. 2017. Quantifying the geomorphic response of modern submarine channels to actively growing folds and thrusts, deep-water Niger Delta. *Geological Society of America Bulletin*, **129**, 1123–1139.

Kane, I.A. and Clare, M.A. 2019. Dispersion, accumulation, and the ultimate fate of microplastics in deep-marine environments: A review and future directions. *Front. Earth Sci.*, **7:80**, <https://doi.org/10.3389/feart.2019.00080>

Kane, I.A., McGee, D.T. and Jobe, Z.R. 2012. Halokinetic effects on submarine channel equilibrium profiles and implications for facies architecture: conceptual model illustrated with a case study from Magnolia Field, Gulf of Mexico. In: Alsop, G.I., Archer, S.G., Hartley, A.J., Grant, N.T. and Hodgkinson, R. (eds) *Salt Tectonics, Sediments and Prospectivity*. Geological Society of London Special Publication, **363**, 289–302.

Kneller, B. 2003. The influence of flow parameters on turbidite slope channel architecture. *Marine and Petroleum Geology*, **20 (6–8)**, 901–910.

Komar, P.D. 1971. Hydraulic jumps in turbidity currents. *GSA Bulletin*, **82 (6)**, 1477–1487.

Konsoer, K., Zinger, J. and Parker, G. 2013. Bankfull hydraulic geometry of submarine channels created by turbidity currents: relations between bankfull channel characteristics and formative flow discharge. *J. Geophys. Res. Earth Surf.*, **118**, 216–228, <https://doi.org/10.1029/2012JF002422>.

Lee, S.E., Talling, P.J., Ernst, G.G.J. and Hogg, A.J. 2002. The occurrence and origin of submarine plunge pools at the base of the US continental slope. *Marine Geology*, **85**, 363–377, [https://doi.org/10.1016/S0025-3227\(01\)00298-5](https://doi.org/10.1016/S0025-3227(01)00298-5)

Lowe, D.R. 1982. Sediment gravity flows II, depositional models with special reference to the deposits of high-density turbidity currents. *Journal of Sedimentary Petrology*, **52**, 279–297.

Macauley, R.V. and Hubbard, S.M. 2013. Slope channel sedimentary processes and stratigraphic stacking, Cretaceous Tres Pasos Formation slope system, Chilean Patagonia. *Marine and Petroleum Geology*, **41**, 146–162, <https://doi.org/10.1016/j.marpetgeo.2012.02.004>

Mayall, M., Lonergan, L., Bowman, A., James, S., Mills, K., Primmer, T., Pope, D., Rogers, L. and Skeene, R. 2010. The response of turbidite slope channels to growth-induced seabed topography. *American Association of Petroleum Geologists Bulletin*, **94**, 1011–1030, <https://doi.org/10.1306/01051009117>

McHargue, T., Pyrcz, M.J., Sullivan, M.D., Clark, J.D., Fildani, A., Romans, B.W. and Drinkwater, N.J. 2011. Architecture of turbidite channel systems on the continental slope: patterns and predictions. *Marine and Petroleum Geology*, **28(3)**, 728–743. <https://doi.org/10.1016/j.marpetgeo.2010.07.008>

Mitchell, N.C. 2006. Morphologies of knickpoints in submarine canyons. *Geological Society of America Bulletin*, **118(5-6)**, 589–605, <https://doi.org/10.1130/B25772.1>

Mitchell, H.W., Whittaker, A.C., Mayall, M., Lonergan, L. and Pizzi, M. 2021. Quantifying the relationship between structural deformation and the morphology of submarine channels on the Niger Delta continental slope. *Basin Research*, **33**, 186–209, <https://doi.org/10.1111/bre.12460>

Morris, P.D., Sylvester, Z., Covault, J.A. and Mohrig, D. 2022. Channel trajectories control deep-water stratigraphic architecture. *The Depositional Record*, **8**, 880-894, <https://doi.org/10.1002/dep2.189>

Mutti, E. and Normark, W.R. 1987. Comparing examples of modern and ancient turbidite systems: problems and concepts. In: Leggett, J.K. and Zuffa, G.G. (eds) *Marine Clastic Sedimentology: Concepts and Case Studies*. Graham and Trotman, London, 1–38.

Palm, F.A., Peakall, J., Hodgson, D.M., Marsset, T., Silva Jacinto, R., Dennielou, B., Babonneau, N. and Wright, T.J. 2021. Width variation around submarine channel bends: Implications for sedimentation and channel evolution. *Marine Geology*, **437**, 106504, <https://doi.org/10.1016/j.margeo.2021.106504>.

Peakall, J. and Sumner, E.J. 2015. Submarine channel flow processes and deposits: A process-product perspective. *Geomorphology*, **244**, 95-120.

Peakall, J., Leeder, M.R., Best, J.L. and Ashworth, P.J. 2000. River response to lateral ground tilting: a synthesis and some implications for the modelling of alluvial architecture in extensional basins. *Basin Research*, **12**, 413-424

Peakall, J., Amos, K.J., Keevil, G.M., Bradbury, P.W. and Gupta, S. 2007. Flow processes and sedimentation in submarine channel bends. *Marine and Petroleum Geology*, **24**, 470-486.

Pettinga, L.A. and Jobe, Z.R. 2020. How submarine channels (re)shape continental margins. *Journal of Sedimentary Research*, **90(11)**, 1581-1600.

Pirmez, C., Beaubouef, R.T., Friedmann, S.J. and Mohrig, D.C. 2000. Equilibrium profile and base level in submarine channels: examples from Late Pleistocene systems and implications for the architecture of deep-water reservoirs. In: Weimer, P., Slatt, R.M., Coleman, J., Rosen, N.C., Nelson, H., Bouma, A.H., Styzen, M.J. and Lawrence, D.T. (eds) *Deep-water Reservoirs of the World*. GCSSEPM Foundation 20th Annual Research Conference Proceedings, 3-6 December, Houston, USA, 782–805.

Pizzi, M., Whittaker, A.C., Mayall, M. and Loneragan, L. 2023. Structural controls on the pathways and sedimentary architecture of submarine channels: New constraints from the Niger Delta. *Basin Research*, **35**, 141–171. <https://doi.org/10.1111/bre.12707>

Shumaker, L.E., Jobe, Z.R., Johnstone, S.A., Pettinga, L.A., Cai, D. and Moody, J.D. 2018. Controls on submarine channel-modifying processes identified through morphometric scaling relationships. *Geosphere*, **14** (5), 2171–2187. doi:10.1130/ges01674.1

Snedden, J.W. 2013. Channel-body basal scours: Observations from 3D seismic and importance for subsurface reservoir connectivity. *Marine and Petroleum Geology*, **39**, 150–163.

Sprague, A.R., Garfield, T.R., Goulding, F.J., Beaubouef, R.T., Sullivan, M.D., Rossen, C., Campion, K.M., Sickafosse, D.K., Abreu, V., Schellpeper, M., Jensen, G.N., Jennette, D.C., Pirmez, C., Dixon, B.T., Ying, D., Ardill, J., Mohrig, D.C., Porter, M.L., Farrell, M.E., and Mellere, D., 2005. Integrated slope channel depositional models: the key to successful prediction of reservoir presence and quality in offshore west Africa (abstract): Colegio de Ingenieros Petroleros de Mexico, cuarto E-Exitep 2005, Veracruz, Mexico, p. 1–13.

Stright, L., Jobe, Z., Fosdick, J.C. and Bernhardt, A. 2017. Modeling uncertainty in the three-dimensional structural deformation and stratigraphic evolution from outcrop data: Implications for submarine channel knickpoint recognition. *Marine and Petroleum Geology*, **86**, 79–94.

Sumner, E.J., Peakall, J., Parsons, D.R., Wynn, R.B., Darby, S.E., Dorrell, R.M., Webb, A. and White, D. 2013. First direct measurements of hydraulic jumps in an active submarine density current. *Geophys. Res. Lett.*, **40**, 5904–5908, <https://doi.org/10.1002/2013GL057862>

Sumner, E.J., Peakall, J., Dorrell, R.M., Parsons, D.R., Darby, S.E., Wynn, R.B., McPhail, S.D., Perrett, J., Webb, A. and White D. 2014. Driven around the bend: spatial evolution and controls on the orientation of helical bend flow in a natural submarine gravity current. *Journal of Geophysical Research – Oceans*, **119**, 898–913. doi: 10.1002/2013JC009008

Sylvester, Z. and Covault, J.A. 2016. Development of cutoff-related knickpoints during early evolution of submarine channels. *Geology*, **44**, 835–838, <https://doi.org/10.1130/G38397.1>.

Sylvester, Z., Pirmez, C. and Cantelli, A. 2011. A model of submarine channel-levee evolution based on channel trajectories: Implications for stratigraphic architecture. *Marine and Petroleum Geology*, **28**, 716–727, <https://doi.org/10.1016/j.marpetgeo.2010.05.012>

Sylvester, Z., Deptuck, M.E., Prather, B.E., Pirmez, C. and O’Byrne, C. 2012. Seismic stratigraphy of a shelf-edge delta and linked submarine channels in the northeastern Gulf of Mexico. In: Prather, B.E., Deptuck, M.E., Mohrig, D., Van Hoorn, B. and Wynn, R.B. (eds) *Application of the Principles of Seismic Geomorphology to Continental Slope and Base-of-Slope Systems: Case Studies from Seafloor and Near-seafloor Analogues*. SEPM Special Publication, **99**, 31–59, <https://doi.org/10.2110/pec.12.99.0031>

Talling, P.J., Masson, D.G., Sumner, E.J. and Malgesini, G. 2012. Subaqueous sediment density flows: depositional processes and deposit types. *Sedimentology*, **59**, 1937–2003, <https://doi.org/10.1111/j.1365-3091.2012.01353.x>

Tek, D.E., McArthur, A.D., Poyatos-Moré, M., Colombera, L., Patacci, M., Craven, B. and McCaffrey, W.D. 2021. Relating seafloor geomorphology to subsurface architecture: How mass transport deposits and knickpoint-zones build the stratigraphy of the deep-water Hikurangi Channel. *Sedimentology*, **68**, 3141– 3190, <https://doi.org/10.1111/sed.12890>

Winter, W.R., Jahnert, R.J. and França, A.B. 2007. Bacia de Campos. *Boletim de Geociências da Petrobras*, **15(2)**, 511–529.

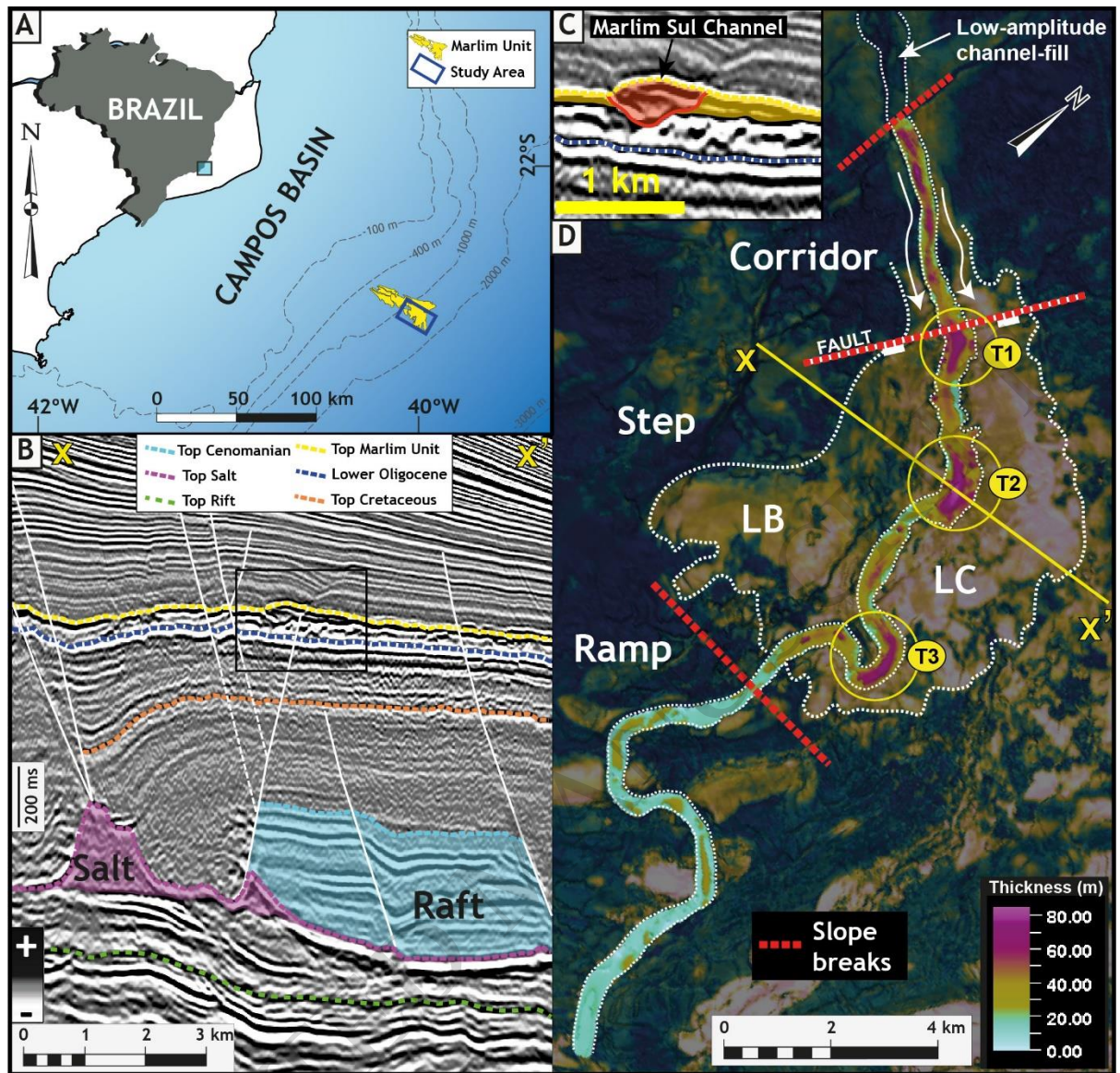


Figure 1

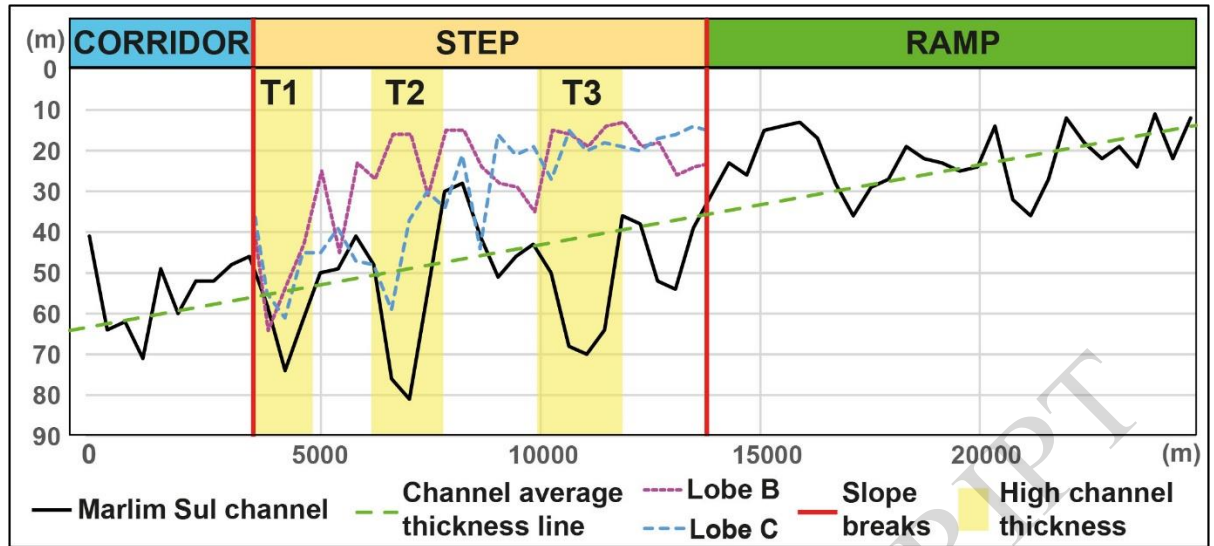


Figure 2

ACCEPTED MANUSCRIPT

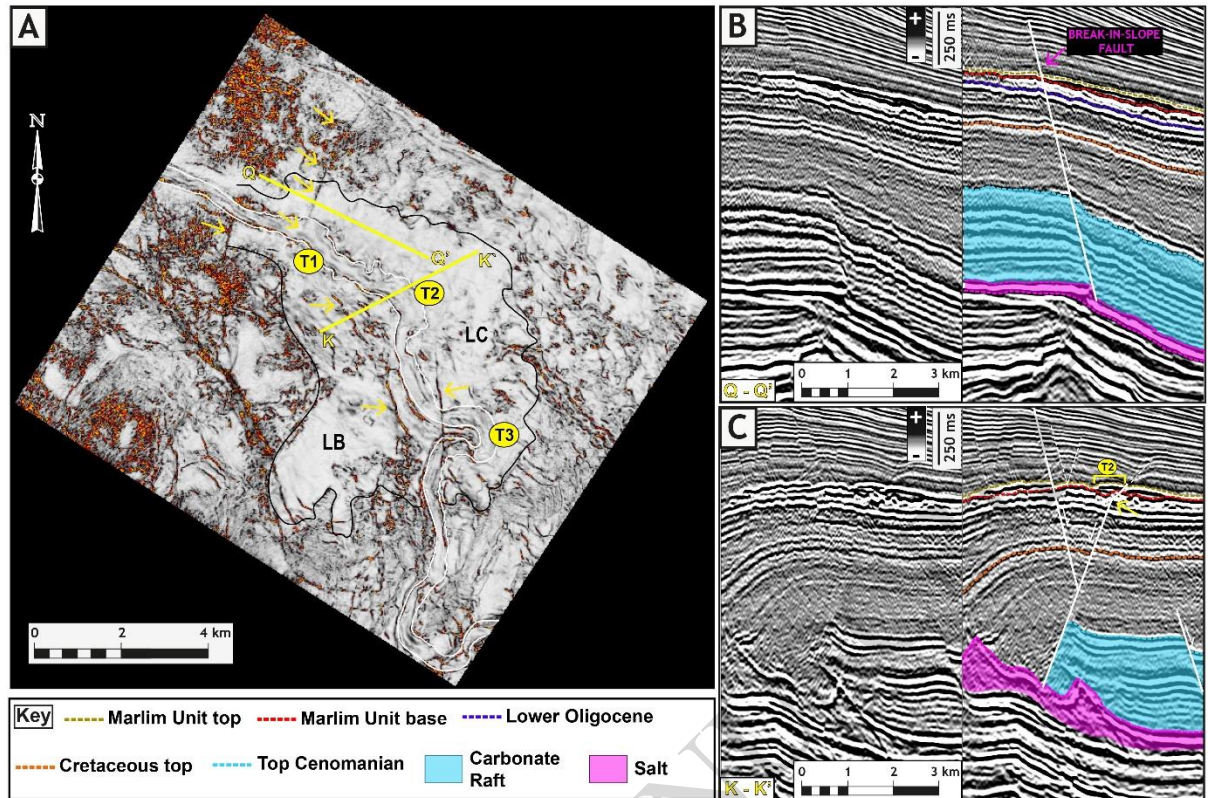


Figure 3

ACCEPTED MANUSCRIPT

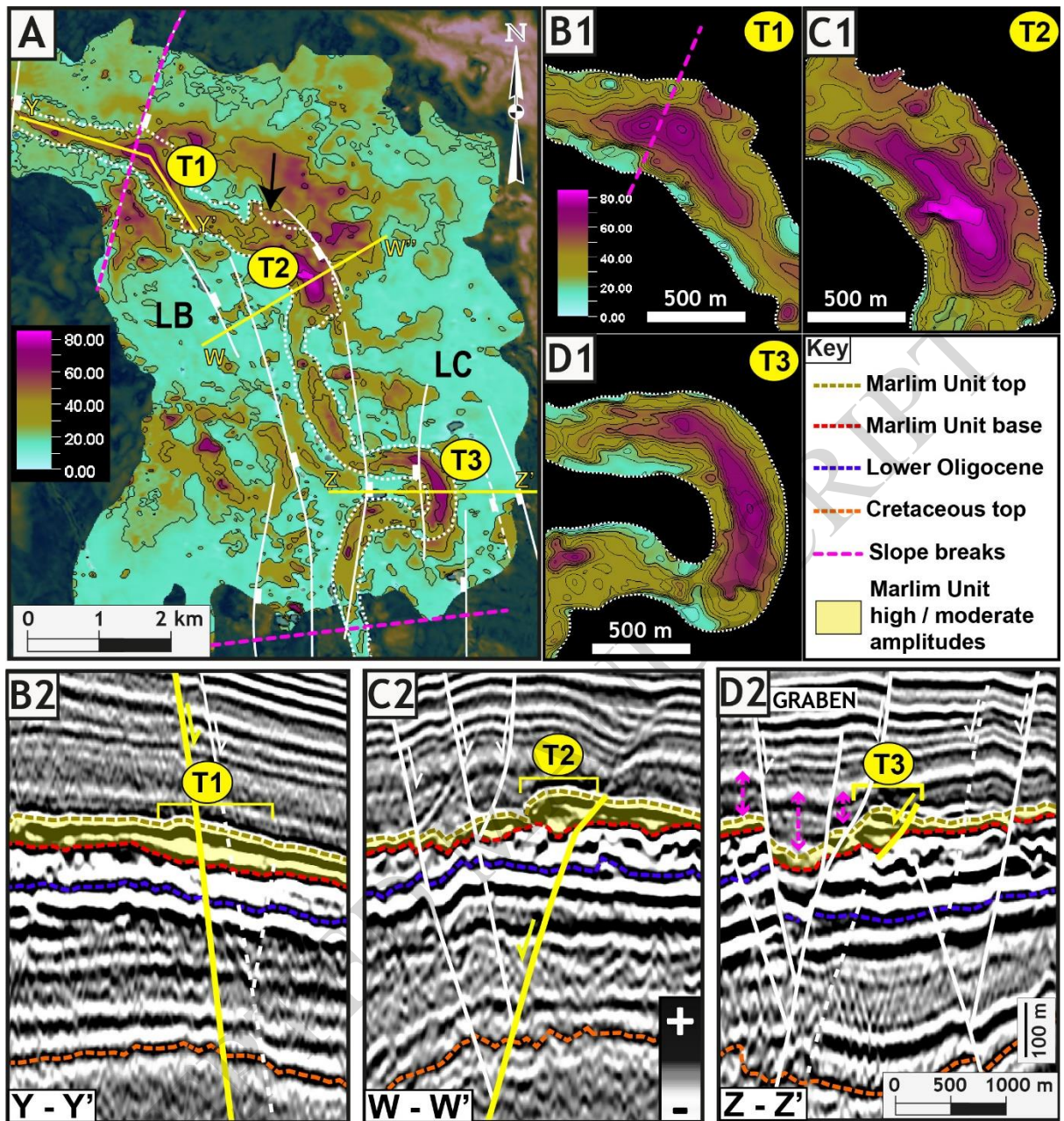


Figure 4

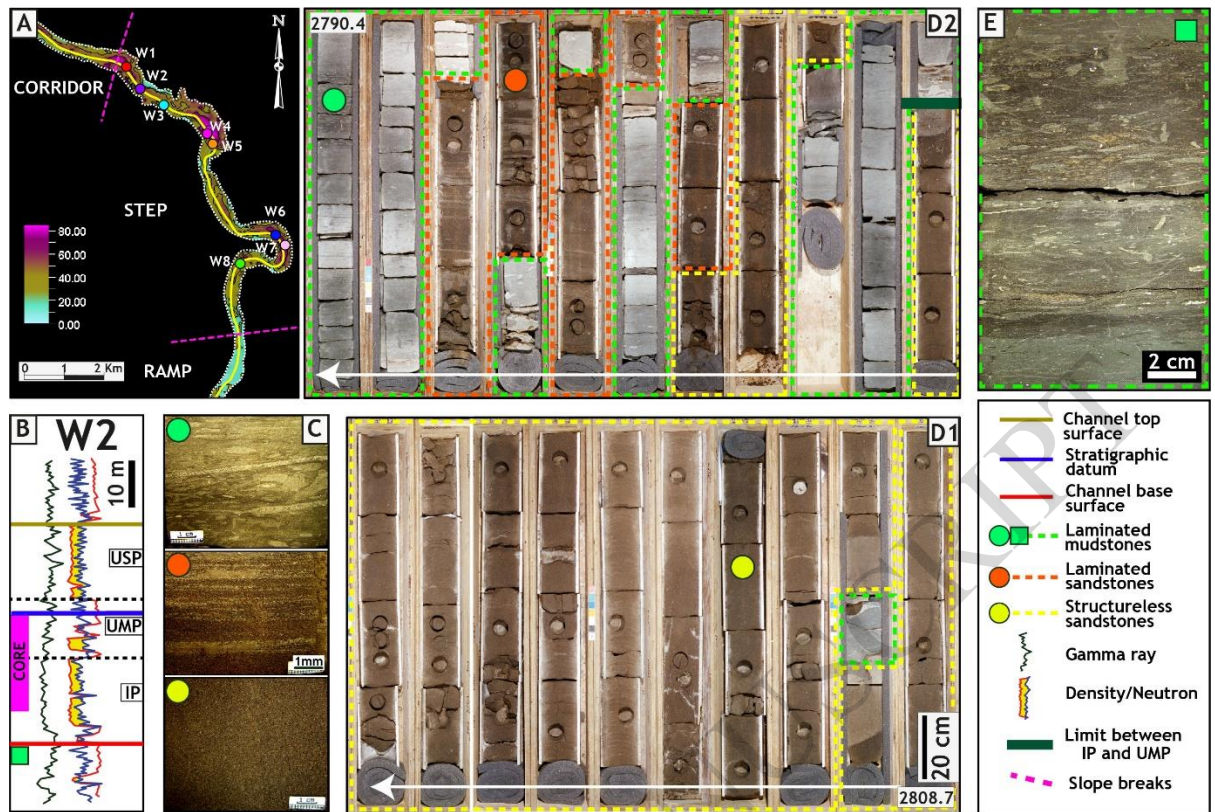


Figure 5

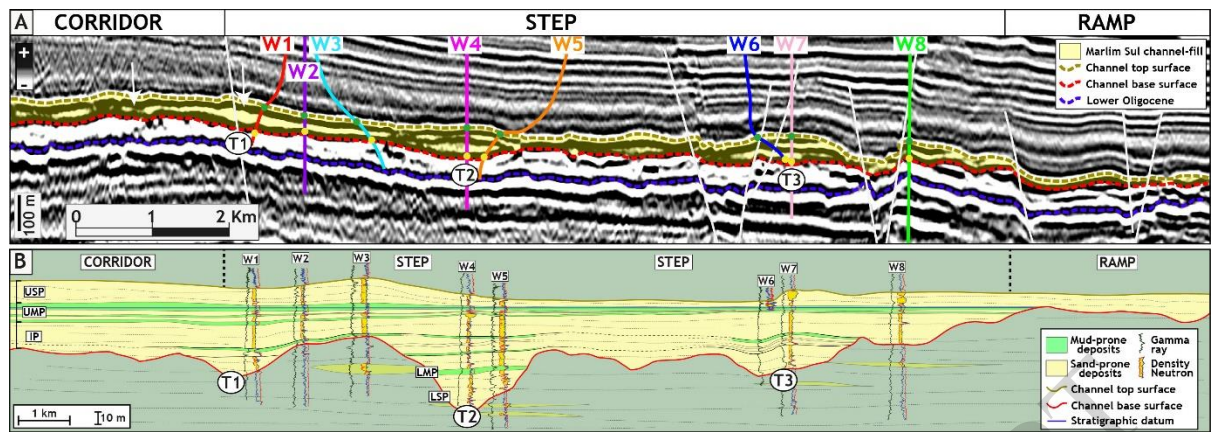


Figure 6

ACCEPTED MANUSCRIPT

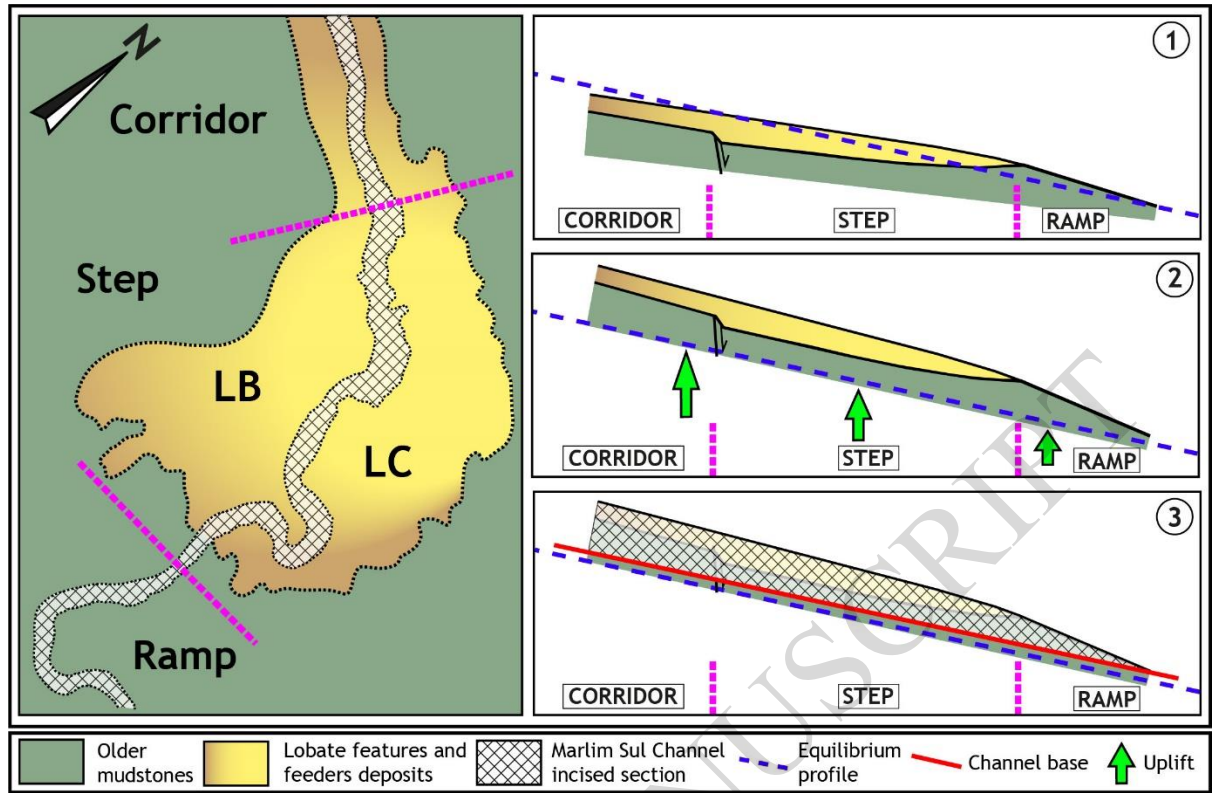


Figure 7